High spin states of ^{91}Mo and ^{89}Nb

Pragya Singh, R. G. Pillay, J. A. Sheikh, and H. G. Devare
Tata Institute of Fundamental Research, Homi Bhabha Road, Bombay 400005, India
(Received 14 April 1993)

In beam γ-ray spectroscopic studies of ^{91}Mo (up to $\frac{33}{2}\hbar$, 6 MeV) and ^{89}Nb (up to $\frac{29}{2}\hbar$, 6.5 MeV) are reported using fusion evaporation reactions with ^{28}Si, ^{30}Si beams and enriched target of ^{66}Zn. The level schemes are well described by spherical shell-model calculations involving neutrons and protons in $1g_{9/2}$ and $2p_{1/2}$ orbitals. The experimentally determined transition probabilities are in reasonable agreement with single particle transition probabilities (Weisskopf estimates).

PACS number(s): 23.20.Lv, 23.20.En, 21.60.Cs, 27.50.+e

I. INTRODUCTION

Recently there has been a surge of interest in the spectroscopic studies of the nuclei in the vicinity of the closed shell $N=50$. Our work on ^{92,90}Mo nuclei [1] has shown that shell-model calculations with protons and neutrons occupying $2p_{1/2}$ and $1g_{9/2}$ give a good description of their level schemes. More exhaustive works on ^{90}Mo by Kabadiyski *et al.* [2] and Arnell *et al.* [3] have shown that the levels up to angular momentum $23\hbar$ and excitation energy of 12 MeV are generated solely by the single-particle excitations in different orbits. A transition to collective behavior was found [4] to set in for ^{87}Mo above 2 MeV excitation energy. Although little is known about the lighter isotopes ^{84,86}Mo which have recently been identified by Gelletly *et al.* [5] and Gross *et al.* [6], the structure of their ground-state bands appears to be rotational-like.

We now report here our findings on ^{91}Mo and ^{89}Nb. Both these nuclei show a striking similarity in their level sequence particularly in the positive parity band. Theoretical shell-model calculations could reproduce the level schemes of ^{91}Mo and ^{89}Nb quite well. In addition, the transition probabilities, as calculated from the experimentally determined lifetimes of some of the states, are in reasonable agreement with the single-particle estimates (Weisskopf estimates).

II. THE EXPERIMENTAL SETUP AND DATA REDUCTION

The experimental measurements consisted of (1) determining the excitation function and recording of gamma-gamma coincidences, (2) the measurement of angular distribution, and (3) finding the lifetimes in picosecond range using the recoil distance method. The measurements were carried out at the Pelletron accelerator facility at Tata Institute of Fundamental Research, Bombay. For the measurement of (1) and (2) a multidetector Compton suppressed spectrometer [7] was utilized and for the measurement (3) a plunger setup [8] was utilized. The spectrometer consisted of 5 HPGe detectors having an energy resolution of 1.9–2.2 keV at 1.33 MeV, each with a transverse type BGO anti-Compton shield, and a multiplicity filter having 8 hexagonal NaI(Tl) (5 cm×10 cm) detectors. The details of the experimental conditions have been described in our earlier work [1].

A. The excitation function and γ-γ coincidence measurements

For the relative excitation function of the γ rays, singles spectra were measured at six energies of the ^{28}Si beam in the heavy-ion fusion reaction ^{66}Zn(^{28}Si;$2pn, 3p2n$)^{91}Mo, ^{89}Nb. Figure 1 shows the relative production cross sections of dominant reaction channels at various beam energies. These cross sections were determined from the yields of their ground-state γ transition. We performed the γ-γ coincidence measurement at 110 MeV beam energy which was chosen with the pur-

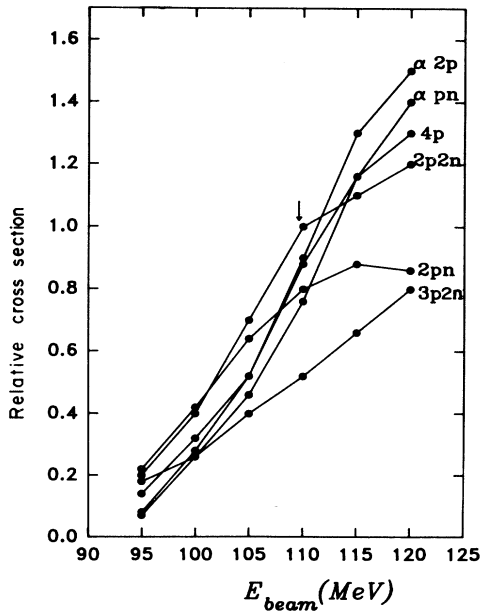

FIG. 1. Plot of the relative cross section for various residues of the reaction ^{28}Si+^{66}Zn. The relative cross sections have been measured with respect to that of the $2p2n$ channel at 110 MeV, marked with an arrow.

pose of achieving optimum cross section for the ^{90}Mo+2p2n reaction [1]. The relative production cross sections of other residual nuclei, such as ^{91}Mo and ^{89}Nb, were found to be appreciable at 110 MeV beam energy. The target used was a 1.4 mg/cm^2 thick ^{66}Zn foil rolled on to a 30 mg/cm^2 of Pb backing. Events corresponding to twofold or higher-fold Ge coincidences along with at least twofold coincidence on the multiplicity filter were recorded in list mode.

The list mode files were recalibrated (0.5 keV/channel) and the background subtracted coincidence spectra were projected for all the detector combinations with gates on all the observed gamma lines. Examples of such coincidence spectra are shown in Fig. 2. Starting from the lowest ground-state transition, all the observed γ lines belonging to the nucleus of interest were identified. The decay scheme was made on the basis of intensity relationships of γ rays in coincidence as well as in singles spectra.

B. The angular distribution measurement

For the angular distribution experiment, we utilized a thin target of thickness 400 μg/cm^2 on a 30 mg/cm^2 Pb backing. The singles spectra gated by twofold or higher-fold coincidence on multiplicity filter were acquired by 5 HPGe detectors placed at 15°, 30°, 44°, 60°, and 90° with respect to the beam direction. For all the γ rays belonging to the nuclei of interest, the measured angular distributions were fitted by the function

$$W(\theta)=\sum_{k=0,2,4} A_k P_k(\cos\theta) \tag{1}$$

where A_k's are the coefficients of Legendre polynomials P_k and θ is the angle of the detector with respect to the beam axis. The fitted values of $A_2^0 \equiv A_2/A_0$, $A_4^0 \equiv A_4/A_0$ were then extracted from the data. The spin and parity assignments to each level were primarily done on the basis of A_2^0 and A_4^0 as described in Ref. [1]. Typical angular distribution curves for dipole and quadrupole transitions are shown in Fig. 3. For some γ lines the A_2^0 and A_4^0 could not be determined accurately due to the presence of contaminating γ lines in the singles spectra obtained in the angular distribution measurements. In such a situation the values of anisotropy ratio were very useful to make correct multipolarity assignment. The so-called "anisotropy ratio," $R_{\rm cal}$, as defined below, was determined from the gamma-gamma coincidence data for all the γ-rays of interest:

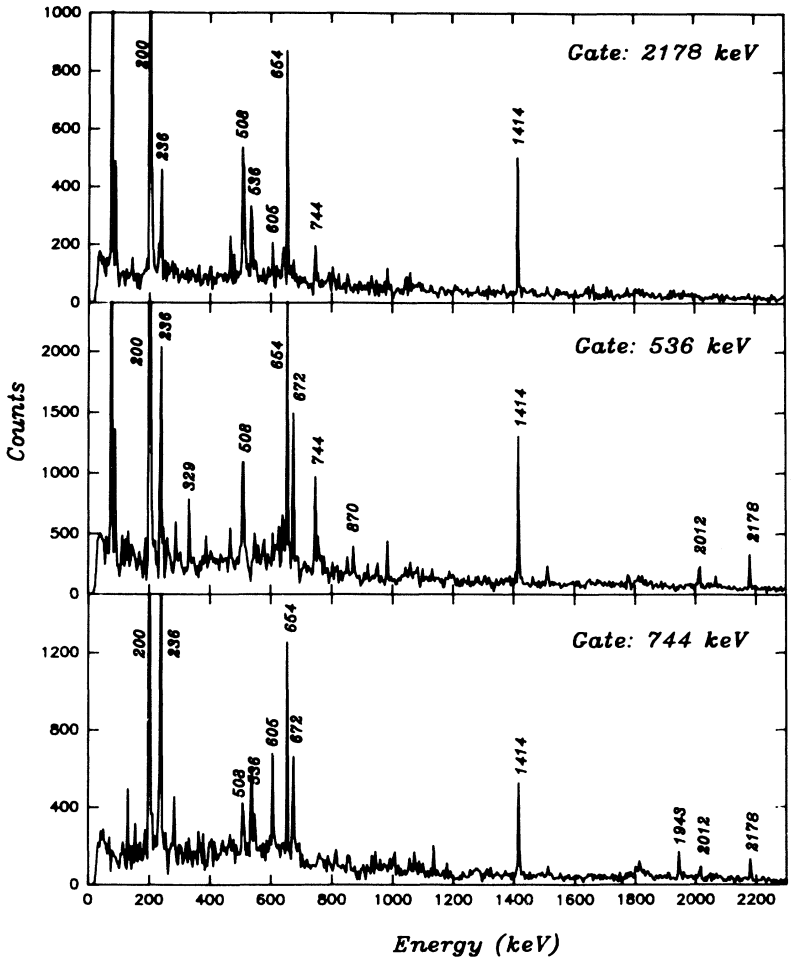

FIG. 2. γ-γ coincidence spectra for ^{91}Mo with gates on γ transitions 2177.8 keV ($25/2^+ \rightarrow 21/2^+$), 535.8 keV ($29/2^+ \rightarrow 27/2^+$), and 744.3 keV ($31/2^+ \rightarrow 29/2^+$).

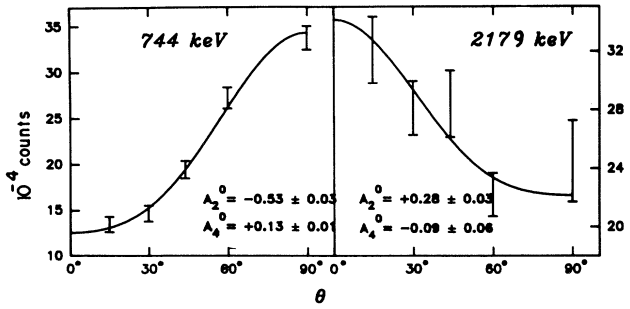

FIG. 3. Representative γ-ray angular distributions observed for a dipole transition ($J+1\rightarrow J$) of energy 744.3 keV, and a quadrupole transition ($J+2\rightarrow J$) of energy 2177.8 keV belonging to ^{91}Mo.

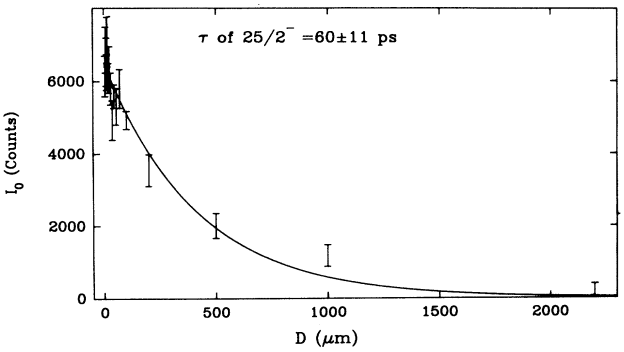

FIG. 4. A plot showing the decay in the intensity of the unshifted component (I_0) of a γ-ray peak as a function of target to stopper separation (D). The mean life (τ) of the state $25/2^-$ of ^{89}Nb was found to be 60±11 ps.

$$R_{\rm cal} = A_{\gamma_1}/B_{\gamma_1} \tag{2}$$

where

$$A_{\gamma_1} = \sum_{\gamma_2} W(\theta_1^{\gamma_1}\theta_2^{\gamma_2}) \text{ with } \theta_1 = 75° \text{ and } \theta_2 = 45° \tag{3}$$

and

$$B_{\gamma_1} = \sum_{\gamma_2} W(\theta_1^{\gamma_1}\theta_2^{\gamma_2}) \text{ with } \theta_1 = 15° \text{ and } \theta_2 = 45° \tag{4}$$

Here $W(\theta_1^{\gamma_1},\theta_2^{\gamma_2})$ is the observed intensity of the transition (γ_1) in the gated (γ_2) spectrum corrected for the efficiency of each detector. Gamma lines with $R_{\rm cal} \geq 1.1$ and $R_{\rm cal} \leq 0.9$ were, respectively, of dipole and quadrupole in character.

C. The lifetime measurement (RDM method)

We performed the lifetime measurement using the plunger setup along with three HPGe detectors placed at −30°, +45°, and 90° with respect to the beam axis. A thin ~380 μg/cm^2 ^{66}Zn target supported by Ta foil of thickness 1.8 mg/cm^2 was used. The target was positioned in a holder such that the Ta side was facing the beam and the holder could be translated relative to the fixed beam stop. The flight distance (D) was varied in the 12–2500 μm range. Two different heavy-ion reactions ^{66}Zn(^{28}Si,2pn)^{91}Mo with beam energy 120 MeV and ^{66}Zn(^{30}Si,$\alpha p2n$)^{89}Nb with beam energy 123 MeV were used.

Singles spectra taken at different distances were normalized not only with the Coulomb excited lines of the Ta stopper, but also with the distance-independent values of I_0 (unshifted peak intensity) for long-lived ($\tau > 1$ ns) transitions. The data were mostly analyzed with the intensities of only the stopped peaks. As the stopper was fixed during the measurement, no solid angle correction was needed for the unshifted peak. The recoil velocities as estimated from the Doppler shift are given below. For the reaction ^{66}Zn(^{28}Si,2pn)^{91}Mo: $\langle v/c \rangle \sim 0.023$. For the reaction ^{66}Zn(^{30}Si,$\alpha p2n$)^{89}Nb: $\langle v/c \rangle \sim 0.025$.

In the analysis of the RDM data, major uncertainties involve the absolute value of D and feeding time due to cascades via higher-lying levels. In determining the mean life (τ) of a given level, it was necessary, therefore, to take explicit account of the lifetimes (τ_i) of those states deexciting to the state of interest. For cases where $\tau_i \ll \tau$, the effect of such feedings is negligible. However, when τ_i is comparable to τ, this feeding must be taken into account. The direct continuum feeding with typical times of about 0.1 ps in this mass region [9] was neglected. Figure 4 shows the decay curve of $25/2^-$ state of ^{89}Nb as an example.

III. EXPERIMENTAL

A. Decay scheme of ^{91}Mo

All the γ lines belonging to ^{91}Mo as revealed by the data analysis are listed in Table I with a summary of other observed properties. The proposed level scheme is presented in Fig. 5. The identification as well as the spin-parity assignment of the states $9/2^+$, $13/2^+$, $17/2^+$, $21/2^+$, $23/2^+$, $25/2^+$, $25/2^-$, and $27/2^-$ are found to be consistent with the published data [10]. However, the γ rays with energies 284.5 and 616.9 keV decaying through states $29/2^-$ and $31/2^-$, as shown in Ref. [10], were found to be wrongly placed. The reason could be that the intensities of these two lines as observed in Ref. [10] were low and both the lines appeared to be essentially of similar intensity. On the other hand, with our experimental results, we have placed them in the level scheme with confidence because of two reasons. First, the intensity of the 616.9 keV line is twice that of the 284.5 keV line. This implies that the 284.5 keV γ ray should correspond to a higher spin state than the state decaying through 616.9 keV γ ray. Second, a new γ ray with energy 340 keV shows coincidence relationship with all the γ rays of energies 616.9 keV, 532.2 keV, etc., down to the 1414.3 keV line, but is not in coincidence with 284.6 keV γ ray (Fig. 5). Thus, with the earlier assignment of $29/2^-$ and $31/2^-$ states as presented in Ref. [10], there is no possible placement consistent with the 340 keV γ ray in that level scheme. In addition to the

TABLE I. Excitation energy (E_x), transition energy (E_γ), relative intensity (I_γ), anisotropy ratio (R_{cal}), angular distribution coefficients (A_2^0, A_4^0), and spin for the states in ^{91}Mo.

E_x [a] (keV)	E_γ [b] (keV)	I_γ	R_{cal}	A_2^0	A_4^0	Assignment J_i^π	Assignment J_f^π
1414.3	1414.3	100.0(16)	0.76(1)	+0.24(3)	−0.07(1)	$13/2^+$	$9/2^+$
2068.3	654.0	99.8(13)	0.84(1)	+0.24(2)	−0.19(1)	$17/2^+$	$13/2^+$
2267.8	199.5	99.9(3)	0.76(1)	+0.33(2)	−0.14(1)	$21/2^+$	$17/2^+$
2940.1	672.3	82.5(12)	1.59(1)	−0.28(2)	+0.01(1)	$23/2^+$	$21/2^+$
3545.2	605.1	28.3(6)	1.48(2)	−0.25(3)	−0.02(1)	$25/2^+$	$23/2^+$
3809.8	869.7	26.7(8)	1.51(3)	−0.23(3)	−0.04(1)	$25/2^-$	$23/2^+$
	265.1	3.2(2)	0.83(1)	+0.26(5)	+0.01(2)	$25/2^-$	$25/2^+$
4342.0	532.2	21.2(3)	1.66(2)	−0.38(3)	+0.09(1)	$27/2^-$	$25/2^-$
4445.6	2177.8	15.7(9)	0.98(7)	+0.28(3)	−0.09(6)	$25/2^+$	$21/2^+$
4953.2	507.6	19.2(3)	1.53(2)	−0.54(3)	+0.09(1)	$27/2^+$	$25/2^+$
	2012.4	8.0(9)	0.73(4)	+0.21(9)	−0.13(7)	$27/2^+$	$23/2^+$
4958.9	616.9	24.3(4)	1.54(2)	−0.51(5)	+0.14(2)	$29/2^-$	$27/2^-$
5243.5	284.6	12.6(2)	1.64(2)	−0.33(3)	+0.07(1)	$31/2^-$	$29/2^-$
5299.1	340.2	11.1(2)	1.52(3)	−0.37(3)	+0.16(1)		$29/2^-$
5489.0	535.8	15.0(4)	1.76(2)	−0.44(4)	+0.14(2)	$29/2^+$	$27/2^+$
	1942.8	10.8(7)	0.75(3)	+0.17(2)	−0.15(6)	$29/2^+$	$25/2^+$
5818.4	329.4	8.2(2)	1.32(2)	+0.07(3)	+0.09(1)		$29/2^+$
6233.3	744.3	20.3(5)	1.45(4)	−0.53(3)	+0.13(1)	$31/2^+$	$29/2^+$
6469.7	236.4	15.8(2)	1.37(2)	−0.47(3)	+0.06(1)	$33/2^+$	$31/2^+$

[a,b]Errors in the energies are ≤ 0.3 keV.

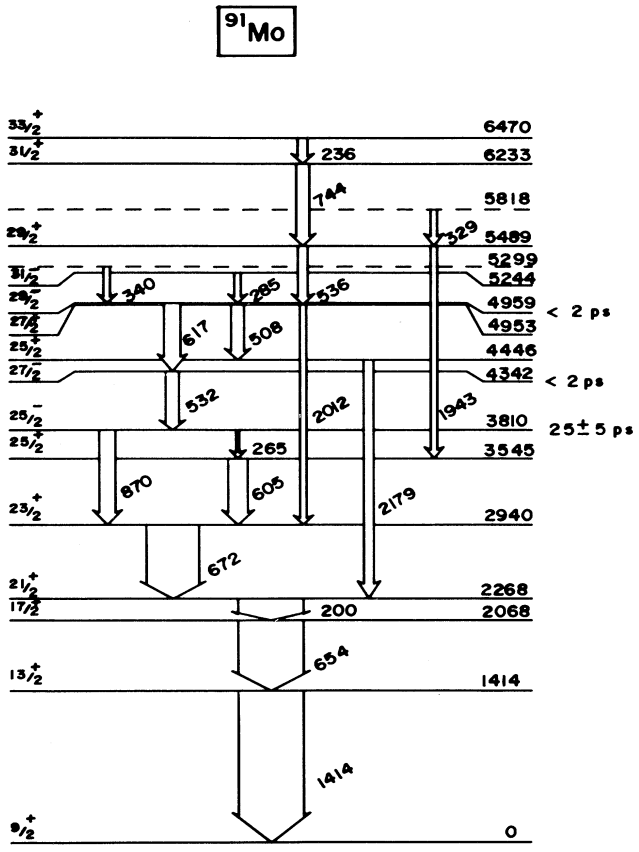

FIG. 5. Level scheme for ^{91}Mo showing excitation energy, γ-transition energies, mean lifetimes and spin values. The γ intensities are roughly proportional to the width of the arrows.

above findings, seven new states decaying through eight γ rays have been established from our experimental results (Fig. 5) but the 211.7 keV transition ($17/2^- \rightarrow 17/2^+$) reported in Ref. [10] was not observed in our data.

From the RDM data, we have determined the lifetime of $25/2^-$ state and made an estimate of the upper limit to the lifetimes of some other states as shown in Fig. 5. The feeding transition 532.2 keV ($27/2^- \rightarrow 25/2^-$) shows all its intensity in the shifted component of the peak even at the lowest measured distance between target and stopper which was 12 μm. Such a separation gives an upper limit to the mean life as 2 ps. From the experimentally determined value of the mean life as 25±5 ps for the state $25/2^-$, the transition probability was calculated to be $\omega_{exp}=(40\pm8)\times10^{14}$ s^{-1}. Assuming the decay $25/2^- \rightarrow 23/2^+$ as pure $E1$, the single-particle estimate of the transition probability ω_{theo} was found to be 13.3×10^{14} s^{-1}. The fairly good agreement between ω_{theo} and ω_{exp}, shows that the contribution of the $M2$ component in the transition $25/2^- \rightarrow 23/2^+$ is very small.

B. Decay scheme of ^{89}Nb

Since ^{89}Nb was not one of the major channels in the fusion reaction studied (Fig. 1), the observed γ lines corresponding to high spin states were very weak. On the basis of our experiment, we established three new levels ($27/2^+$, $29/2^+$, $29/2^-$) and placed many transitions (Fig. 6) in the level scheme complementing the earlier work on ^{89}Nb [11]. Table II summarizes the observed properties of the γ rays.

Similar to the case of ^{91}Mo, the RDM data for ^{89}Nb were utilized to determine the lifetime of a state or to find

TABLE II. Excitation energy (E_x), transition energy (E_γ), relative intensity (I_γ), anisotropy ratio (R_{cal}), angular distribution coefficients (A_2^0, A_4^0) and spin for the states in ^{89}Nb.

E_x [a] (keV)	E_γ [a] (keV)	I_γ	R_{cal}	A_2^0	A_4^0	Assignment J_i^π	J_f^π
1003.7	1003.7	100.0(16)	0.83(1)	+0.27(2)	−0.12(1)	$13/2^+$	$9/2^+$
1935.4	931.7	84.0(14)	0.78(1)	+0.25(3)	−0.24(1)	$17/2^+$	$13/2^+$
2151.5	216.1	18.9(3)	0.69(2)	+0.28(3)	−0.05(1)	$17/2^-$	$17/2^+$
2193.0	257.6	44.0(4)	0.86(1)	+0.35(2)	−0.14(1)	$21/2^+$	$17/2^+$
2956.0	763.0	24.5(6)	1.29(2)	−0.31(3)	−0.07(1)	$23/2^+$	$21/2^+$
3142.6	991.1	43.1(6)	0.87(1)	−0.06(4)	−0.14(2)	$21/2^-$	$17/2^-$
3403.3	447.3	17.6(5)	1.62(2)	−0.41(3)	−0.02(1)	$25/2^+$	$23/2^+$
3806.1	402.8	19.8(6)	1.44(2)	−0.14(2)	+0.08(1)	$25/2^-$	$25/2^+$
	663.0	10.4(4)	0.98(2)	+0.14(3)	−0.02(1)	$25/2^-$	$21/2^-$
4554.3	748.2	14.5(5)	1.33(1)	−0.53(3)	+0.07(1)	$27/2^-$	$25/2^-$
4809.1	254.8	6.9(2)	1.78(3)	−0.31(3)	+0.06(1)	$29/2^-$	$27/2^-$
5042.3	1639.0	9.5(8)	0.93(2)	−0.02(2)	−0.02(2)	$27/2^+$	$25/2^+$
6101.3	1059.0	2.3(9)				$(29/2^+)$	$27/2^+$

[a]Errors in the energies are ≤ 0.3 keV.

its upper limit. As is apparent from Fig. 6, the lifetime of the state $25/2^-$ could be determined through the exponential decay of either the 663 keV γ ray or the 403 keV γ ray. We obtained 60 ± 11 ps as the lifetime of the $25/2^-$ state consistently through both the decay paths. We note from Table II that the intensity ratio (branching ratio) of 663 and 403 keV transition is nearly 0.5. Since the value of the branching ratio is the same as the ratio of their transition rates, the transition rates were found to be 5.6×10^9 s^{-1} and 11.2×10^9 s^{-1} for 603 and 403 keV decay paths, respectively. Since the decay $25/2^-\rightarrow21/2^-$ (663 keV transition) is pure $E2$, the con-

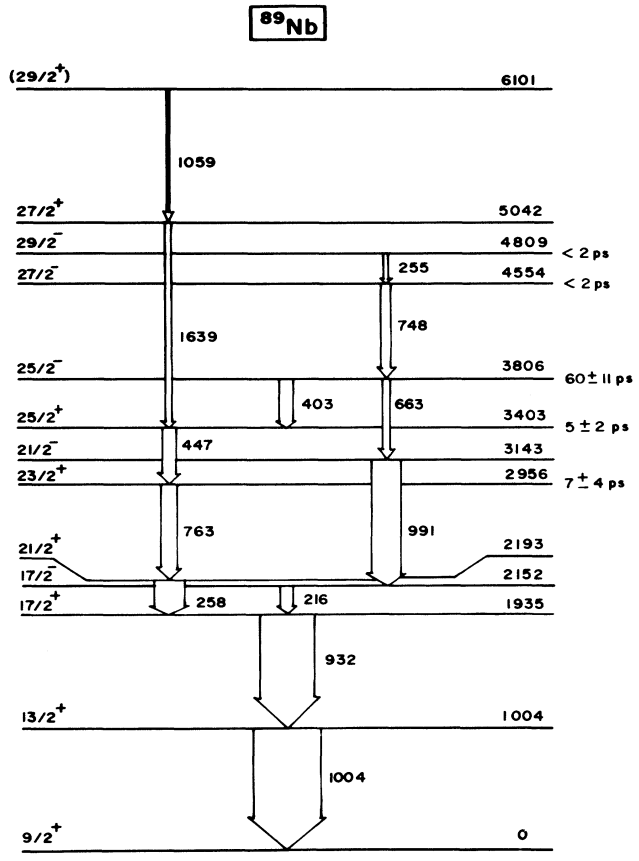

FIG. 6. Level scheme for ^{89}Nb showing excitation energy, γ-transition energies, mean lifetimes, and spin values. The γ intensities are roughly proportional to the width of the arrows.

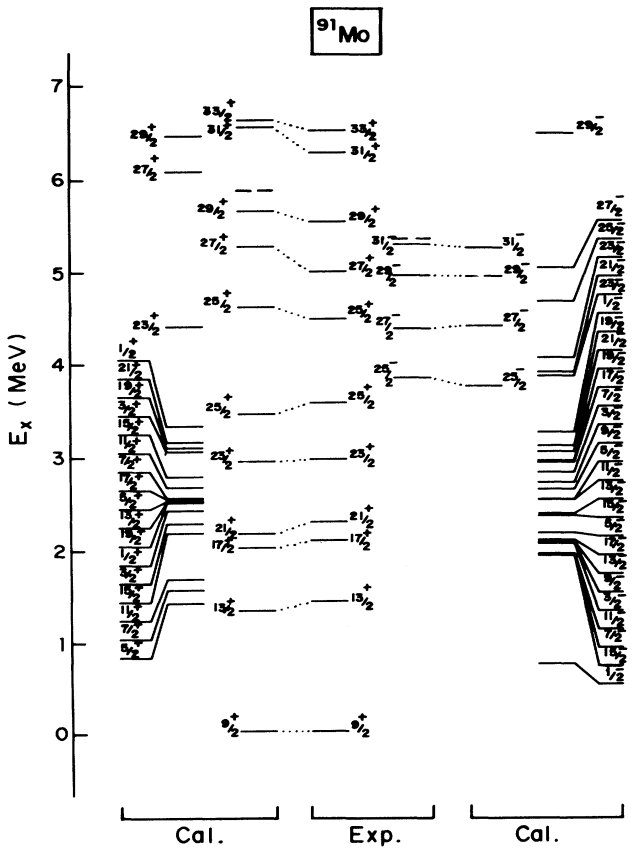

FIG. 7. Comparison of the observed states in ^{91}Mo with shell-model calculations within the $(2p_{1/2}, 1g_{9/2})$ model space.

sistency between single-particle estimate of the transition probability (ω_{theo}) and the experimentally determined value (ω_{exp}) can be easily checked. There was indeed a good agreement between ω_{theo} ($=3.7\times10^{9}$ s^{-1}) and ω_{exp} [$=(5.5\pm1.4)\times10^{9}$ s^{-1}].

Assuming the appropriate values of the feeding lifetime to the states $25/2^{+}(25/2^{+}\rightarrow23/2^{+})$ and $23/2^{+}(23/2^{+}\rightarrow21/2^{+})$, their mean lifetimes were determined to be 5 ± 2 ps [$\omega_{exp}=(1.4\pm0.7)\times10^{11}$ s^{-1}] and 7 ± 4 ps [$\omega_{exp}=(2\pm1)\times10^{11}$ s^{-1}], respectively. since there can be mixing of $M1$ and $E2$ in both these transitions, the values of mixing ratios are required to calculate the single-particle estimates of their transition probability. In fact, the value of ω_{exp} for both these states lies between the Weisskopf estimates for pure $M1$ and for pure $E2$ transitions.

IV. THEORETICAL STUDY

We performed the shell model calculations [12,13] for ^{89}Nb and ^{91}Mo with valence protons and neutrons occupying the $(2p_{1/2}, 1g_{9/2})$ configuration space keeping ^{88}Sr as the inert core. These calculations were carried out in the neutron-proton product formalism with the Hamiltonian represented by

$$H = H_{pp} + H_{nn} + H_{np} \tag{5}$$

where $H_{pp,H_{nn}}, H_{pn}$ are the effective interaction between the valence protons, valence neutron holes, among proton and neutron hole, respectively. The 33 parameters [four single particle (hole) energies, nine matrix elements of the proton-proton effective interaction, and twenty matrix elements of the proton-neutron hole two-body effective

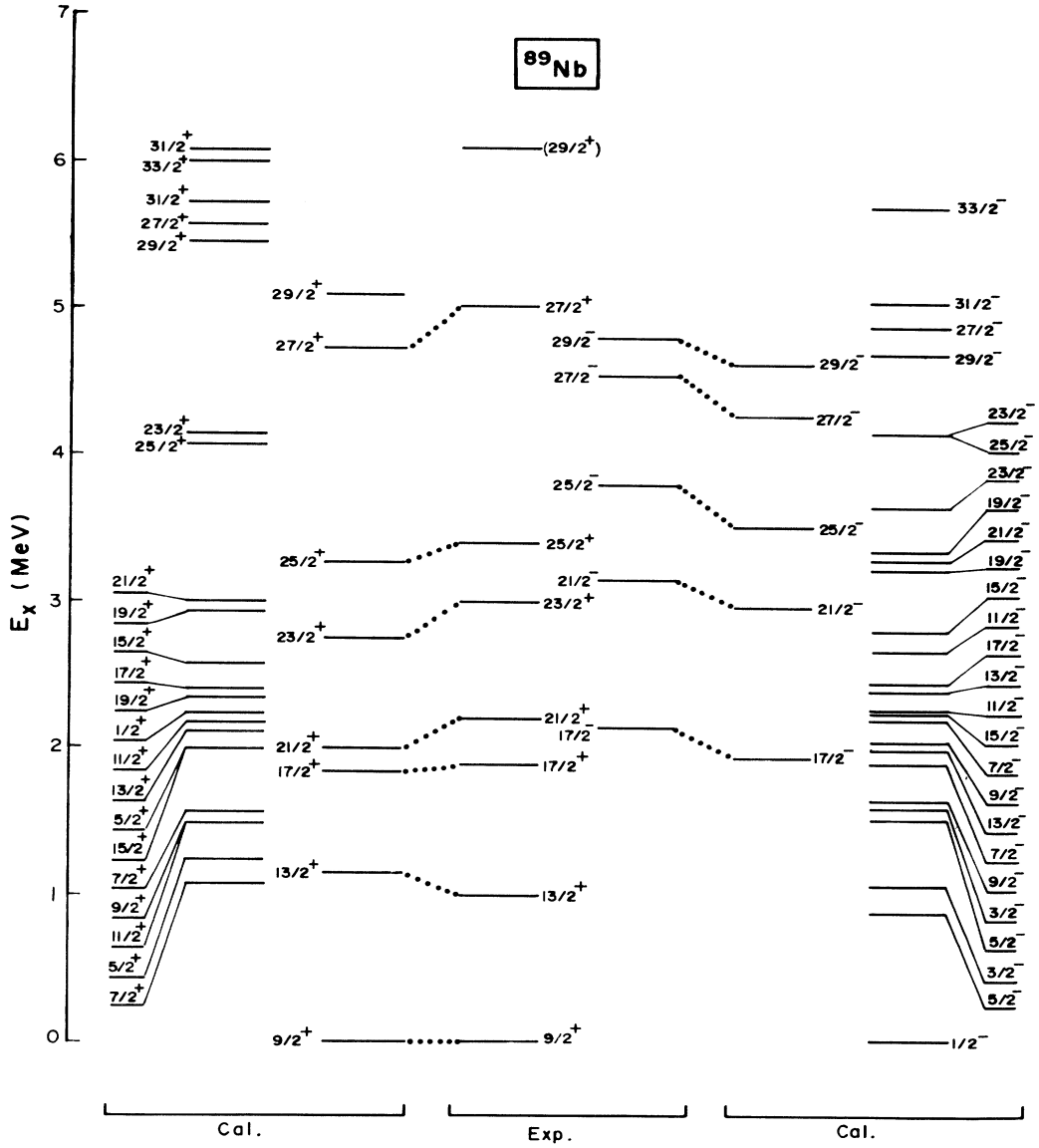

FIG. 8. Comparison of the observed states in ^{89}Nb with shell-model calculations within the $(2p_{1/2}, 1g_{9/2})$ model space.

interaction] define the above Hamiltonian completely. These parameters have been obtained in a least squares fit to the observed spectra of ^{90}Zr, ^{91}Nb, ^{92}Mo,^{93}Tc, and ^{94}Ru with $N=50$, ^{88}Y, ^{89}Zr, ^{90}Nb, ^{91}Mo with $N=49$ and ^{86}Sr with $N=48$ [13].

The shell model level scheme thus obtained reproduced the experimental data very well for ^{91}Mo (Fig. 7). The states up to $25/2^-$ and $27/2^-$ were employed in the fitting procedure so it is not surprising to see a good agreement between the two. The calculated states above $J=25/2^+$ and $27/2^-$ are predictions and are also seen to agree fairly well with the corresponding experimental levels obtained in the present work.

The shell-model wave function in the neutron-proton coupled representation is given by

$$\psi_J^i = \sum_{\nu_p J_p \nu_n J_n} C^i_{(\nu_p J_p)(\nu_n J_n)J} (\phi_{\nu_p J_p} \otimes \phi_{\nu_n J_n})_J \qquad (6)$$

where $\nu_{p(n)}$ denotes the seniority quantum numbers for protons (neutrons) and label the basis states uniquely for particle numbers ≤ 3 in $1g_{9/2}$ orbital. As expected, the ground state $J=9/2^+$ is a $\nu_n=1$ state. The $J=13/2^+$, $17/2^+$, $21/2^+$, and the lowest $25/2^+$ have predominantly $\nu(\equiv\nu_p+\nu_n)=3$ components. The second observed $25/2^+$ state is predominantly a $\nu=5$ state with the dominant components $[J_p=8,9,10,12(\nu_p=4)$; $J_n=9/2(\nu_n=1)]$ with a fair amount of $\nu=3$ components. The presence of the $\nu=3$ contribution pushes this state towards the lower side on the energy scale. The higher spin states above $J=25/2^+$ are entirely $\nu=5$ states.

Figure 8 shows that the shell-model level scheme of ^{89}Nb compares well with the experimentally observed levels. The matching is particularly striking since none of the ^{89}Nb levels was employed in determining the interaction matrix elements and the single particle energies. The states $J=13/2^+,17/2^+,21/2^+,23/2^+$, and $25/2^+$ have $\nu=3$. The top two positive parity states $(27/2^+,29/2^+)$ have $\nu=5$. The lowest negative parity state $J=17/2^-$ is a mixture of $\nu=3$ and 5 configurations and higher spin states are purely $\nu=5$ states.

V. DISCUSSION AND CONCLUSION

The irregular spacing of levels in the decay schemes of both the nuclei studied here clearly indicated the single-particle nature of the level scheme. In addition, the experimentally determined values of the transition probabilities of some states agree fairly well with the single-particle estimates. The theoretical shell-model calculation with valence nucleons in $2p_{1/2}$ and $1g_{9/2}$ orbits could reproduce the spectra quite well. In the case of ^{91}Mo, the highest observed spin states $33/2^+$ and $31/2^-$ are, in fact, the maximum angular momentum values which could be generated by the model space considered in the shell-model calculations. There is a noticeable similarity between the level sequence of the positive parity band in ^{91}Mo and ^{89}Nb (Fig. 9). We explain this by assuming the charge independent nature of the nucleon-nucleon interactions and noting that both ^{91}Mo and ^{89}Nb have the same number of valence nucleons outside the inert core ^{88}Sr—4 proton particles and 1 neutron hole for ^{91}Mo, and 3 proton particles and 2 neutron holes for ^{89}Nb. There were very few yrast negative parity states observed to make such a comparison.

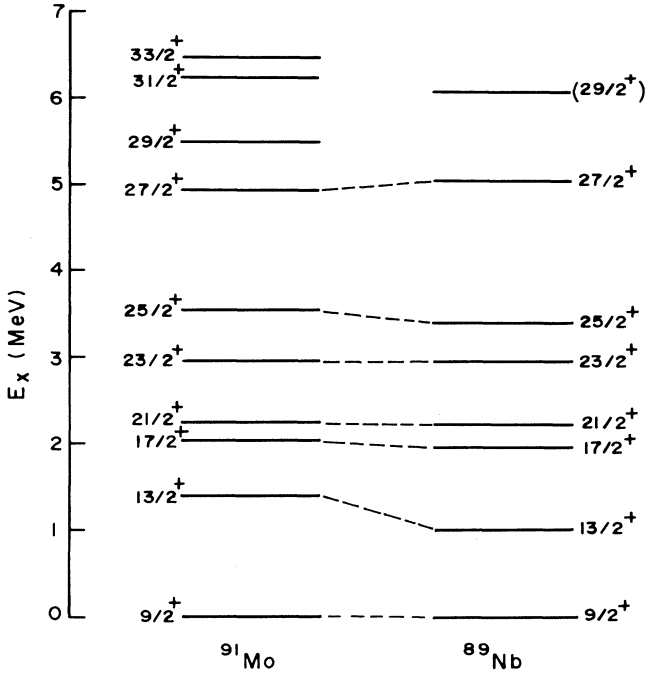

FIG. 9. Comparison of experimentally found positive parity states of ^{91}Mo with those of ^{89}Nb.

We conclude that the observed properties of ^{91}Mo and ^{89}Nb give no indication for the existence of any collective motion of the nucleus. On the other hand, the experimentally observed spin states in both these nuclei could be well explained by shell-model calculations.

ACKNOWLEDGMENTS

The authors wish to thank Professor H. C. Jain and S. Chattopadhyay for the use of RDM setup and their help in the lifetime measurement and R. S. Chakrawarthy for data analysis. The computer program NSCSORT used here for fitting the γ peaks was kindly provided by Dr. R. Bhowmik of Nuclear Science Centre, New Delhi, India.

[1] P. Singh, R. G. Pillay, J. A. Sheikh, and H. G. Devare, Phys. Rev. C **45**, 2161 (1992).

[2] M. K. Kabadiyski, F. Cristancho, C. J. Gross, A. Jungclaus, K. P. Lieb, D. Rudolph, H. Grawe, J. Heese, K. H. Maier, J. Eberth, S. Skoda, W. T. Chou, and E. K. Warburton, Z. Phys. A **343**, 165 (1992).

[3] S. E. Arnell, D. Foltescu, H. A. Roth, Ö. Skeppstedt, A. Nilsson, S. Mitarai, and J. Nyberg, Physica Scripta **46**, 389

(1992).
[4] Ch. Winter, D. J. Blumenthal, P. Chowdhury, B. Crowell, P. J. Ennis, C. J. Lister, C. J. Gross, J. Heese, A. Jungclaus, K. P. Lieb, J. Eberth, and S. Skoda, Phys. Lett. B **258**, 289 (1991).
[5] W. Gelletly, M. A. Bentley, H. G. Price, J. Simpson, C. J. Gross, J. L. Durell, B. J. Varley, Ö. Skeppstedt, and S. Rastikerdar, Phys. Lett. B **253**, 287 (1991).
[6] C. J. Gross, W. Gelletly, M. A. Bentley, H. G. Price, J. Simpson, K. P. Lieb, D. Rudolph, J. L. Durell, B. J. Varley, and S. Rastikerdar, Phys. Rev. C **44**, R2253 (1991).
[7] P. Singh, Ph.D. thesis, University of Bombay, 1992 (unpublished).
[8] H. C. Jain, S. Chattopadhyay, Y. K. Agarwal, M. L. Jhingan, S. K. Mitra, H. V. Panchal, and A. Roy, Pramana **37**, 269 (1991).
[9] H. P. Hellmeister, K. P. Lieb, and W. Müller, Nucl. Phys. **A307**, 515 (1978).
[10] A. Nilsson and M. Grecescu, Nucl. Phys. **A212**, 448 (1973).
[11] K. Oxorn, S. K. Mark, J. E. Kitching, and S. S. M. Wong, Z. Phys. **A321**, 485 (1985).
[12] D. H. Glockner and F. J. D. Serduke, Nucl. Phys. A **220**, 477 (1974).
[13] R. Gross and A. Frenkel, Nucl. Phys. **A267**, 85 (1976).